Solid-State Electronics 207 (2023) 108712

Contents lists available at ScienceDirect

Solid State Electronics

journal homepage: www.elsevier.com/locate/sse

Liquid-gate 2D material-on-insulator transistors for sensing applications ☆

Carlos Marquez *, Elsa Fuente-Zapico, Paula Martinez-Mazon, Jose C. Galdon, Luca Donetti, Carlos Navarro, Francisco Gamiz

Nanoelectronics Research Group (CITIC-UGR), Department of Electronics, University of Granada, 18071, Granada, Spain

ARTICLE INFO

Keywords:
Graphene
2D materials
Biosensors
Reliability
Liquid-gate transistor
Inter-gate coupling

ABSTRACT

This research investigates the use of 2D materials (specifically graphene) as active channel in liquid-gate transistors used as detectors of biological targets on functionalized surfaces. However, before these sensors can be effectively used, it is crucial to establish a reliable sensing platform within two-dimensional materials as active channels, and to evaluate the fabrication, lithography, and reliability of these devices. In this study, we analyzed the inter-device variability and reliability of the transistors, as well as the potential factors that may exacerbate these issues under operative conditions. We performed structural characterization to confirm the quality of the materials, followed by photolithography and processing to create liquid-gate sensors. We then conducted electrical evaluations of the devices, which revealed significant reliability issues and inter-device variability. To address these problems, we propose the use of an intergate-coupling effect that utilizes both front- and back-gates simultaneously. Our findings have important implications for the design and optimization of 2D materials-based liquid-gate sensors for biological applications.

1. Introduction

Graphene, a single-atom layer of carbon, has emerged as a highly promising material for next-generation electronic devices [1]. Its atomic thickness and high surface-to-volume ratio enable excellent electrical and thermal transport properties, precise electrostatic control, and high sensitivity to environmental changes, making it an ideal candidate for biosensing applications [2–5]. Electrochemical studies have shown that the ions accumulate at the surface of graphene when a gate voltage is applied between the electrodes, without charge transferred across the interface [6]. These studies suggest that graphene operates nearly as an ideal polarized electrode [7,8]. The graphene–electrolyte interface is typically modeled as an electrical double layer capacitance (EDLC), constituted by two layers of ions that are created at the surface of graphene. The first layer is composed of ions of opposite charges to those present in the graphene, and the second layer is composed of positive and negative charged ions that progressively reach the potential of the solution far from the graphene surface. The EDLC can be modulated applying a voltage at a reference electrode immersed in the electrolyte solution, controlling the number of free carriers in graphene, and therefore its conductivity. The minimum of free carriers and thus the minimum of conductivity is reached when the Fermi level coincides with the energy where the conduction and valence bands merge. The gate bias where this condition is fulfilled is known as the Dirac point. While electrochemical gated sensors using electrolytes such as ionic liquids and aqueous solutions have been widely explored for biological recognition [9,10], repeatability and device variability issues pose significant challenges, particularly with respect to the sensitivity of graphene and the complex nature of electrolyte solutions [11]. In this study, we aim to assess the impact of device variability and reliability on the feasibility of using graphene-based sensors for biosensing. We conduct a comprehensive evaluation of several sensor devices using both structural and electrical characterization methods. To mitigate variability issues, we adopt a double-gate structure that enables us to gain insights into the factors that influence sensor instability, such as interface traps and defects, and reduce inter-device variability.

2. Experimental setup

Graphene was synthesized through low-pressure chemical vapor deposition (LPCVD) where polycrystalline copper foil was used as catalytic substrate. The reaction was made at 1 Torr using methane (CH_4) as a carbon precursor. Later, the graphene layers were transferred to patterned Si/SiO_2 substrates using the PMMA based technique [12]. To pattern the metal pads on the substrates before the graphene transfer, Cr (10 nm)/Au (100 nm) electrodes were deposited by physical vapor deposition. In order to remove any PMMA residues and clean the

☆ The review of this paper was arranged by Sorin Cristoloveanu.

* Corresponding author.
E-mail address: carlosmg@ugr.es (C. Marquez).

https://doi.org/10.1016/j.sse.2023.108712

Available online 20 July 2023

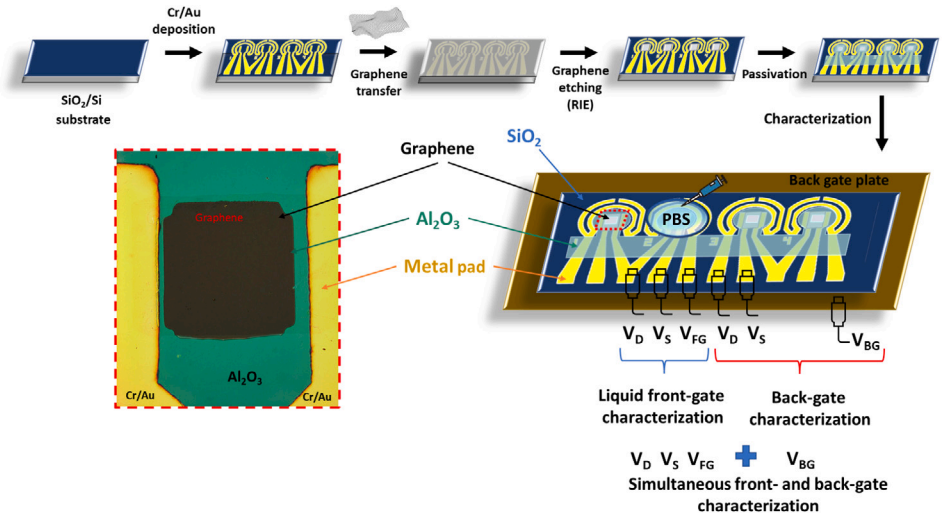

Fig. 1. Scheme of the fabrication, processing, and characterization of the graphene-on-insulator transistors.

graphene surface, the samples were then annealed in a furnace at 350 °C in an Ar/H_2 atmosphere for 1 h. After graphene deposition, reactive-ion etching (RIE) at 10 W and 30 sccm of O_2 was used to remove the graphene outside the devices channel. Finally, the devices were partially passivated using deposited Al_2O_3 in a lift-off photolithography process to avoid any potential drain/source shortcut when the liquid gate is employed (green color in device picture at Fig. 1). Up to four sensors sharing the back SiO_2/Si structure were fabricated. The device fabrication process is summarized in the top part of Fig. 1.

For the structural characterization, Raman and X-ray Photoelectron Spectroscopy (XPS) microscopy were used. Raman spectra were measured in a Witec alpha300 equipment at 532 nm laser excitation. The laser power was set to 20 mW and an objective of 100x and 600 l per mm were used. All spectra were accumulated for 50 times. XPS was performed using a Kratos Axis Ultra-DLD spectrometer with Al Kα (1486.6 eV) radiation.

Regarding the electrical characterization, semiconductor analyzer (Keysight B1500) and temperature- and pressure-controlled probe stations (Süss PA-300PS and Janis cryostat) were employed. Three different characterization techniques were carried out. To have information about the graphene/back-gate interface, transfer (I_{DS}-V_{BG}), output (I_{DS}-V_{DS}) and transient (I_{DS}-t) characteristics of the devices were measured without any liquid and using a back-gate setup (Fig. 1, red bracket). The Si in the Si/SiO_2 structure (acting as the back-gate) is accessible through a common back-gate plate. To evaluate the electrochemical characteristics of the devices, a phosphate buffered saline solution (PBS) at a 0.001x concentration was placed covering the graphene to perform the liquid gate. Thanks to the Al_2O_3 passivation, source and drain contacts are isolated from the liquid avoiding any potential conductive path with the PBS (Fig. 1, blue bracket). Finally, an electrical characterization using both front- and back-gate interfaces were employed (Fig. 1, bottom part) to determine the potential intergate-coupling characteristic of the fabricated devices.

3. Results and discussion

Developing a sensing platform that requires repeatability and reliability necessitates material corroboration and the identification of potential sources of variability. From the structural characterization point of view we have developed Raman and X-ray photoelectron spectroscopy. Fig. 2.a displays the components in the C 1s spectra of the XPS characteristic for one of the devices. Binding energies were referenced to the C 1s peak at 285 eV. The fitting of the C 1s peak using a Gaussian–Lorentzian deconvolution shows the C–C peak (~285 eV), C-O-C (~286.5 eV), and C(=O)-O (~288.8 eV) peaks. These results are in agreement with the expected for pristine CVD graphene [13]. To corroborate the quality and the variability in number of layers along the fabricated material, Raman characterization in Fig. 3 displays the characteristic spectra at various points on the surface for two different fabricated devices. The Raman spectrum of the graphene device exhibited the characteristic G peak (1580 cm^{-1}) and 2D peak (~2665 cm^{-1}), along with a small D peak (~1330 cm^{-1}) associated with the defects [14]. The low-intensity band observed at 2455 cm^{-1} (2LO) in all samples resulted from a nondispersive second-order longitudinal optical phonon induced by the excitation laser [15]. Notably, the ratio of G to 2D peaks and the amplitude of D peaks differed depending on the measuring point. These results demonstrate that, despite high-quality synthesized graphene, areas with two- or multi-layer characteristic can be present along the channel.

The transfer characteristic (I_{DS}-V_{GS}) for a graphene-liquid gate transistor was initially characterized using a PBS 0,001x solution as a front-gate. To determine the reliability of the devices both double swept and repeated measurements (3) were conducted. As observed in Fig. 3.a, consecutive measurements of the device showed a small shift in the current. However, this shift tended towards zero after the third measurement (not shown). The device also exhibited a significant hysteresis, with drain current differing when the gate voltage was swept downward (from 1.2 V to −0.5 V) compared to when it was biased upward (from −0.5 V to 1.2 V). This hysteresis could not be attributed to gate current leakage, as the gate current was much smaller (around three orders of magnitude) than the drain current (dashed lines in Fig. 3). To further explore this hysteresis, Fig. 3.b shows the transient response of the device. This is a current-time characterization for a specific gate bias (V_{FG} = 0,4 V for this case). As observed, the temporal signature of the drain–source current presents two different trends: an increase in the current for the first seconds of operation and a subsequent decrease. Please notice the semi log scale. The time to reach the maximum in the temporal signature could be associated with the mobile ions forming the double layer capacitance (EDLC) which also implies a shift in the Dirac voltage (gate bias for the current minimum) to the left. This behavior also produces a decrease of the gate current, observed at the same time. The second phenomenon observed as a drain–source current decrease (not noticeable in the gate current), can be associated with the bias instabilities associated with trap and defect related effects and commonly observed in semiconductors [16]. Both these phenomena contribute to the observed hysteresis (including a crossing point) in the transfer characteristic.

Fig. 4.a shows the case of the transfer characteristic for several sensors when using the liquid front-gate configuration. A considerable

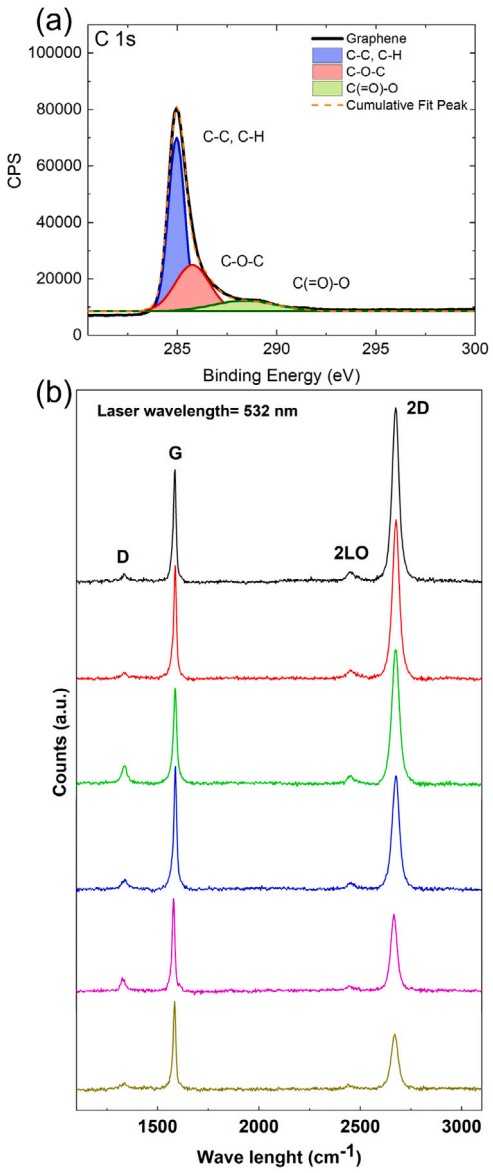

Fig. 2. (a) XPS spectrum of the C1s peak for a graphene device and, (b) Raman spectra for different points on two different devices.

inter-device variability is observed, being the standard deviation for the eight devices around the 40% of the mean value of the Dirac voltage. This value could suppose a critical aspect for a potential sensing application. The case of a back-gate configuration (without liquid-gate) is shown in Fig. 4.b for the same devices. In this case, the Dirac voltage variability is also important but lower in percentage according to the standard deviation and mean values. However, in the temporal response (Fig. 4.b inset), the drain current follows the same behavior as the front-gate configuration (Fig. 3.b), but in this case without the presence of any liquid (no EDLC formation) and with negligible current through the back-gate. This result points that the initial phenomenon has its origin in the graphene or at its interfaces (maybe due to the expected high density of states, ions and impurities after the liquid-involved graphene processing and transfer) and discards difficulties or delays to form the EDLC layer.

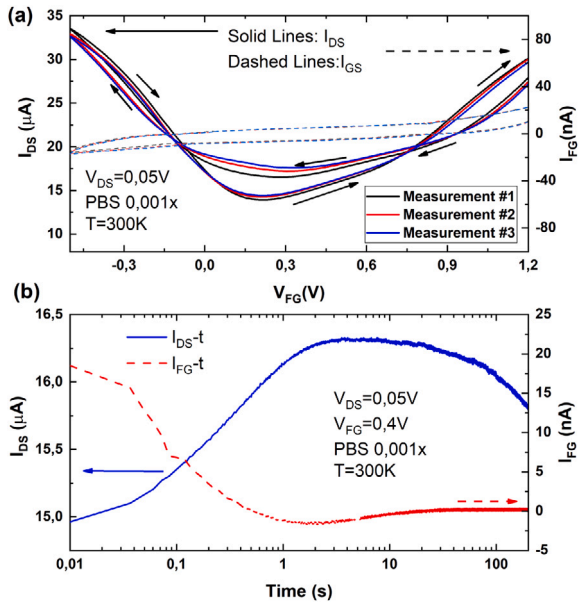

Fig. 3. (a) I_{DS}-V_{GS} characterization in double voltage sweep for a graphene liquid-gate sensor (solid lines) for three repeated measurements when PBS is employed as a front-gate. (b) Temporal response of the device. Gate currents are included in the right axis.

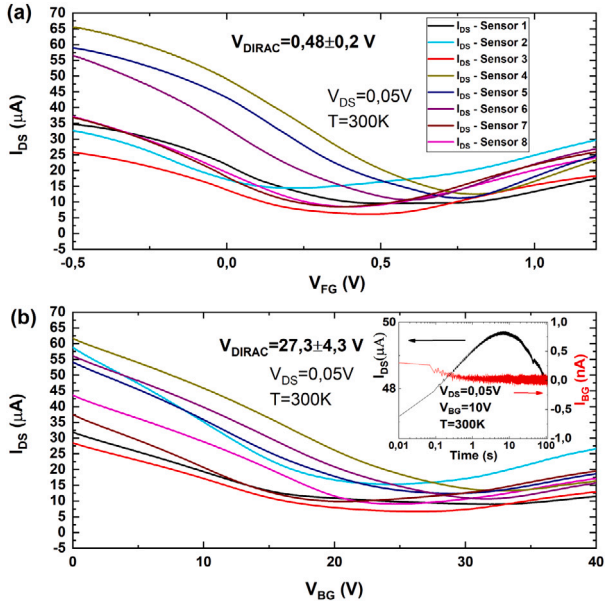

Fig. 4. (a) I_{DS}-V_{FG} characterization for several graphene sensors using the liquid front-gate configuration. (b) I_{DS}-V_{BG} characterization for the same graphene sensors but using the back-gate configuration. Temporal response for the drain and the back-gate currents of one device is included in the inset.

Due to the presumable high density of defects and impurities after the sensor fabrication (despite the annealing), to achieve reliable sensing platform, alternatives have to be explored. Fig. 5 shows the case of performing a simultaneous front- and back-gate biasing configuration. Increasing the back-gate voltage, thanks to the inter-gate coupling, there is a Dirac voltage shift toward to higher voltages. With this configuration, around a 14% of modulation of the Dirac voltage is achievable sweeping the back-gate voltage in a range from 0 to 40 V. This effect can open the doors to set particular back-gate voltages

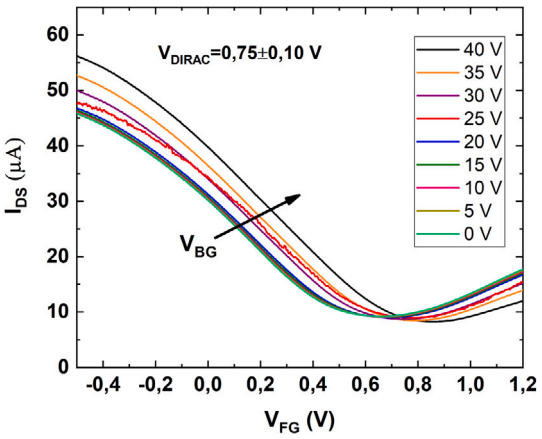

Fig. 5. I_{DS}-V_{FG} for a sensor as a function of back-gate voltage.

on each sensor depending on its specific Dirac voltage to reduce the inter-device variability.

4. Conclusion

The outcome of this work provides further insight on the inter-device variability and reliability observed when dealing with graphene liquid-gate sensors. The presence of the same reliability issues when only using back-gate discards that observed variability could have its origin in the liquid gate operation. Moreover, the electro-coupling between the front- and the back-gate opens the door to set particular back-gate voltages to reduce the variability and the reliability issues observed after several measurements.

Declaration of competing interest

The authors declare that they have no known competing financial interests or personal relationships that could have appeared to influence the work reported in this paper.

Data availability

Data will be made available on request.

Acknowledgments

This work has received funding from the European Union's Horizon 2020 research and innovation programme under the MSC grant No 895322 and from the Spanish and Andalusian Programs DTS20/00038, P18-RT-4826, PYC-020-RE-023UGR, A-TIC-628-UGR20 and PID2020-119668GB-I00. Funding for open access charge: Universidad de Granada / CBUA

References

[1] Novoselov KS, Fal ko VI, Colombo L, Gellert PR, Schwab MG, Kim K. A roadmap for graphene. Nature 2012;490(7419):192–200.

[2] Lee CW, Suh JM, Jang HW. Chemical sensors based on two-dimensional (2D) materials for selective detection of ions and molecules in liquid. Front Chem 2019;7(November):1–21, URL https://www.frontiersin.org/article/10.3389/fchem.2019.00708/full.

[3] Liu Y, Dong X, Chen P. Biological and chemical sensors based on graphene materials. Chem Soc Rev 2012;41:2283–307. http://dx.doi.org/10.1039/C1CS15270J.

[4] Kochmann S, Hirsch T, Wolfbeis OS. Graphenes in chemical sensors and biosensors. TRAC Trends Anal Chem 2012;39:87–113, New Materials in Analytical Chemistry, URL https://www.sciencedirect.com/science/article/pii/S016599361200194X.

[5] Liu M, Zhang W, Chang D, Zhang Q, Brennan JD, Li Y. Integrating graphene oxide, functional DNA and nucleic-acid-manipulating strategies for amplified biosensing. TRAC Trends Anal Chem 2015;74:120–9, URL https://www.sciencedirect.com/science/article/pii/S0165993615002253.

[6] Valota AT, Kinloch IA, Novoselov KS, Casiraghi C, Eckmann A, Hill EW, et al. Electrochemical behavior of monolayer and bilayer graphene. ACS Nano 2011;5(11):8809–15, URL https://pubs.acs.org/doi/10.1021/nn202878f.

[7] Dankerl M, Hauf MV, Lippert A, Hess LH, Birner S, Sharp ID, et al. Graphene solution-gated field-effect transistor array for sensing applications. Adv Funct Mater 2010;20(18):3117–24, URL https://onlinelibrary.wiley.com/doi/10.1002/adfm.201000724.

[8] Du X, Guo H, Jin Y, Jin Q, Zhao J. Electrochemistry investigation on the graphene/electrolyte interface. Electroanalysis 2015;27(12):2760–5, URL https://onlinelibrary.wiley.com/doi/10.1002/elan.201500302.

[9] Chen F, Qing Q, Xia J, Li J, Tao N. Electrochemical gate-controlled charge transport in graphene in ionic liquid and aqueous solution. J Am Chem Soc 2009;131(29):9908–9.

[10] Liu N, Chen R, Wan Q. Recent advances in electric-double-layer transistors for bio-chemical sensing applications. Sensors (Switzerland) 2019;19(15).

[11] Ávila J, Galdon JC, Recio MI, Salazar N, Navarro C, Marquez C, et al. Improved inter-device variability in graphene liquid gate sensors by laser treatment. Solid-State Electron 2022;192(January).

[12] Borin Barin G, Song Y, de Fátima Gimenez I, Souza Filho AG, Barreto LS, Kong J. Optimized graphene transfer: Influence of polymethylmethacrylate (PMMA) layer concentration and baking time on graphene final performance. Carbon 2015;84(C):82–90, URL https://linkinghub.elsevier.com/retrieve/pii/S0008622314011269.

[13] Ederer J, Janoš P, Ecorchard P, Tolasz J, Štengl V, Beneš H, et al. Determination of amino groups on functionalized graphene oxide for polyurethane nanomaterials: XPS quantitation vs. functional speciation. RSC Adv 2017;7(21):12464–73.

[14] Ferrari AC, Robertson J. Interpretation of Raman spectra of disordered and amorphous carbon. Phys Rev B 2000;61:14095–107, URL https://link.aps.org/doi/10.1103/PhysRevB.61.14095.

[15] Wallace JS, Quinn A, Gardella JA, Hu J, Kong ES-W, Joh H-I. Time-of-flight secondary ion mass spectrometry as a tool for evaluating the plasma-induced hydrogenation of graphene. J Vac Sci Technol B, Nanotechnol Microelectron: Mater, Process, Meas Phenom 2016;34(3):03H113. http://dx.doi.org/10.1116/1.4942086.

[16] Marquez C, Salazar N, Gity F, Navarro C, Mirabelli G, Galdon JC, et al. Investigating the transient response of schottky barrier back-gated mos_2 transistors. 2D Mater 2020. URL https://iopscience.iop.org/article/10.1088/2053-1583/ab7628.